# Tumor SNR Analysis in Scintimammography by Dedicated High Contrast Imager

Maria Nerina Cinti, Roberto Pani, *Member, IEEE,* Rosanna Pellegrini, Claudio Bonifazzi, Raffaele Scafè, Giuseppe De Vincentis, Franco Garibaldi, Francesco Cusanno, Renato Campanini, Nico Lanconelli, Alessandro Riccardi, and Alberto del Guerra, *Senior Member, IEEE*

***Abstract*—A new gamma camera dedicated to scintimammography (single photon emission mammography—SPEM) now has a full-breast field of view. One can clinically examine a mildly compressed breast with a cranio-caudal-like projection as one would in X-ray mammography. This camera is based on pixelated scintillation arrays and position sensitive photomultiplier tubes. By reducing the collimator-tumor distance, we enhanced the geometric spatial resolution and the contrast. Unfortunately, due to the low counting rates in scintimammography, low contrast images are usually seen, particularly with small tumors.**

**The aim of this paper is to evaluate how a camera, based on a pixelated detector, can improve the SNR values for small tumors by effectively correcting the spatial response. The procedure is based on good pixel identification. We used a small gamma camera with a metal channel dynode position sensitive photomultiplier (Hamamatsu R7600-C8) coupled to different CsI(Tl) scintillator arrays with a general purpose collimator. This type of photomultiplier drastically reduces the charge spread and improves the intrinsic characteristics of the imager. The dimensions of the CsI (Tl) matched the photomultiplier's active area ($22 \times 22$ mm$^2$). Utilizing its very high intrinsic spatial resolution, we created a look up table to correct gain and spatial nonuniformities. We used a breast and torso phantom to characterize the SNR as a function of pixel size, thickness of the breast, tumor size, and depth.**

**The data showed that the SNR depends principally on the match between the tumor and pixel size. For instance, for a 6 mm diameter tumor, the best SNRs were obtained by a $2 \times 2$ mm$^2$ array. For larger tumors, up to 10 mm diameter, a larger pixel $3 \times 3$ mm$^2$ or $4 \times 4$ mm$^2$, optimizes the SNR value. We compared the results of this camera with those from both a SPEM gamma camera and a standard Anger camera.**

***Index Terms*—Biomedical nuclear imaging, photomultipliers, scintillation detectors.**

Manuscript received January 14, 2002; revised April 14, 2003. This work was supported in part by the MIUR Cofin 2000 Project.

M. N. Cinti is with the Graduate School of Biophysics, Department of Biochemical Science, University of Rome, La Sapienza, 00161 Rome, Italy (e-mail: marianerina.cinti @uniroma1.it).

R. Pani, R. Pellegrini, and G. De Vincentis are with the Department of Experimental Medicine and Pathology, University of Rome, La Sapienza, 00161 Rome, Italy.

C. Bonifazzi is with the Department of Human Physiology, University of Ferrara, 44100 Ferrara, Italy.

R. Scafè is with ENEA TEC, CR, Casaccia, 00060 Rome, Italy.

F. Garibaldi and F. Cusanno are with the Laboratory of Physics, ISS, 00100 Rome, Italy.

R. Campanini, N. Lanconelli, and A. Riccardi are with the Department of Physics, University of Bologna, 40126 Bologna, Italy.

A. del Guerra is with the Department of Physics, University of Pisa, 56126 Pisa, Italy.

Digital Object Identifier 10.1109/TNS.2003.817345

## I. Introduction

STANDARD scintimammographic breast images are usually acquired with an Anger camera (AC), using the radiopharmaceutical $^{99m}$Tc Sestamibi, with the patient in a prone position. This technique has been shown to provide high sensitivities and specificities (>95%) for tumors larger than 1 cm. However, for smaller tumors the sensitivities were considerably lower (40–50%) [1]. The introduction of a new 5 in, full-breast field of view (FoV), gamma camera dedicated to scintimammography (single photon emission mammography—SPEM) [2]–[4], allows a clinical examination with the breast mildly compressed in the cranio-caudal projection, equivalent to the same view in X-ray mammography. This camera is based on pixelated scintillation arrays and position sensitive photomultiplier tubes (PSPMTs).

The reduction of the collimator-tumor distance enhanced the geometric spatial resolution and contrast. Furthermore, by combining this technique with a higher intrinsic spatial resolution detector it was possible to enhance sensitivity up to 80% for <1 cm tumor size [5]. Unfortunately, due to the low counting rates in scintimammography, low contrast images are usually seen, particularly with small tumors.

The aim of this paper is to investigate those characteristics of these imaging systems that allow further enhancement of image contrast and signal-to-noise ratio (SNR), specifically for small tumor detection. An imaging system such as the Anger camera, which is based on a single large planar detector, has intrinsic resolution that is worse than the collimator resolution for a short distance from the surface of the collimator. In addition the coarse digitization of the image (3.2 mm usually) places an additional limit on the resolution and contrast. In this study, we plan to evaluate how a camera based on a pixellated detector and PSPMT can improve image contrast and SNR for small tumors by an effective correction for the spatial response Our hypothesis is that, thanks to effective pixel identification, it is possible to produce a correspondence between image digitalization and scintillator crystal lattice that can enhance image contrast. To demonstrate this, we analyzed the performance of a small gamma camera with good pixel identification, comparing the tumor SNR with those obtained for an Anger Camera and a 5 in gamma camera based on scintillator array (SPEM). Monte Carlo simulations were also performed to help understand the results.

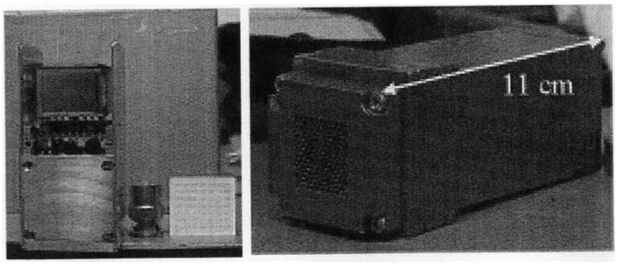


Fig. 1. SGC. On the left, lateral view of gamma camera, with photomultiplier and electronic device; on the right, lead housing and collimator.

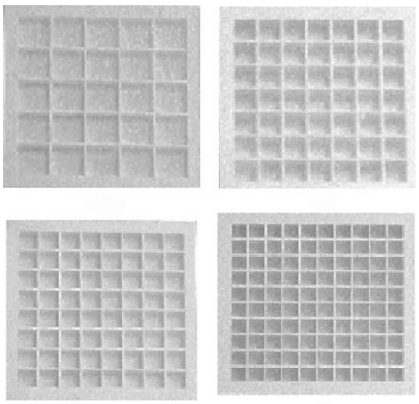

Fig. 2. CsI (Tl) crystals. From left upper corner, clockwise: $5 \times 5$ pixels, $4.2 \times 4.2 \times 5\ mm^3$; $7 \times 7$ pixels, $3 \times 3 \times 5\ mm^3$, $10 \times 10$ pixels, $2 \times 2 \times 5\ mm^3$, $8 \times 8$ pixels, $2.5 \times 2.5 \times 5\ mm^3$.

## II. Equipment and Method

### A. Small Gamma Camera (SGC)

The small gamma camera consisted of a parallel hole collimator, a CsI(Tl) scintillating array, and a Hamamatsu R7600-C8 PSPMT as shown in Fig. 1.

We tested a number of CsI (Tl) scintillating arrays with an active area of $22 \times 22\ mm^2$. The crystals were 5 mm thick, the dead zone was 0.25 mm wide, and the single crystal sizes ranged from $2.0 \times 2.0\ mm^2$ to $4.2 \times 4.2\ mm^2$. The crystals were chosen so that there were an integer number of pixels for the same area (see Fig. 2). The area corresponded to the PSPMTs active area.

The Hamamatsu R7600-C8 PSPMT (Bialkali photocathode) [4] is a compact, metal channel dynode PMT with readouts by row ($4X + 4Y$). The active area is $22 \times 22\ mm^2$ and the overall dimensions are $26 \times 26 \times 20$(h) $mm^3$. The camera is made of eight preamplifiers directly connected to each wire anode. A weighted summing circuit was built to compute the charge distribution centroid.

The acquisition system consisted of a FAST 7074 analog-to-digital converter (ADC) module connected to a FAST multiparameter acquisition system operating in the Windows environment (MPA/WIN). We used an MPA acquisition card in a Pentium personal computer. The multiparameter system was able to control up to eight ADCs with a maximum count rate of 400 KHz. The maximum electronics count rate was 30 KHz. The data were acquired in list mode through a 1 Mbyte first-in–first-out register (FIFO) inside the MPA card. We developed software to process and elaborate data for the image analysis.

TABLE I
Collimator Characteristics

| Camera | Collimator | Sensitivity | Spatial Resolution FWHM SCD (mm) | | | Hole diameter (mm) | Hole length (mm) | Septal Thickness (mm) |
|---|---|---|---|---|---|---|---|---|
| | | | 0 | 50 | 100 | | | |
| Anger | General Electric General Purpose H2503DF | 362 cpm/μCi[a] (0.163 cts/kBq) | 2.5 | 6 | 9 | 2.5 | 41 | 0.3 |
| SPEM & SGC | NUCLEAR fields (The Netherlands) General Purpose | 327 cpm/μCi[b] (0.147 cts/kBq) | 2.3 | 5.7 | 8.8 | 1.5 | 22 | 0.2 |

[a] Value for NaI(Tl) _ at 100 mm SCD ( source-collimator distance)
[b] Value for CsI(Tl) array, 3 mm thickness at 100 mm SCD

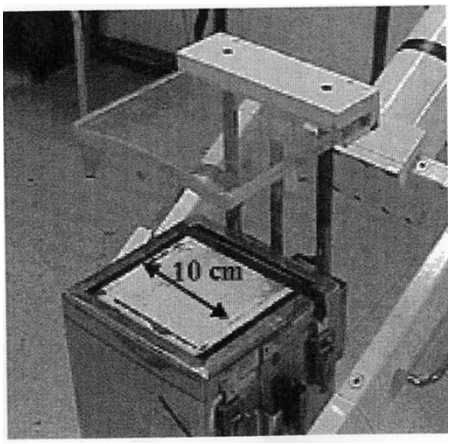


Fig. 3. SPEM camera.

TABLE II
Energy and Intrinsic Spatial Resolution

| Camera | Energy resolution FWHM | Spatial resolution % FWHM |
|---|---|---|
| ANGER | 11 % | 3.5 mm |
| SPEM | 21 % | 1.7 mm |

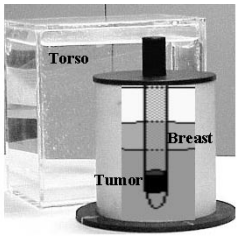


Fig. 4. Breast and torso phantoms. The draw shows one possible position of the tumor inside the breast phantom.

We used a standard nuclear field, low energy, all purpose collimator (see Table I).

### B. SPEM and Anger Camera

The SPEM consisted of a 5 in Hamamatsu PSPMT R3292 coupled to a 5 in diameter CsI (Tl) scintillating array with $2 \times 2 \times 3\ mm^3$ pixels. The collimator was the same as that of the SGC (see Fig. 3). A detailed description of the SPEM camera is reported elsewhere [2]. The AC was a standard General Electric (GE) Starcam with a GE H2503DF collimator (see Table I). The energy resolution and the intrinsic spatial resolution for both cameras are summarized in Table II. We obtained the energy

resolution values for the SPEM Camera after a correction of the pulse height uniformity response by using a lookup table based on the spectra acquired on each pixel of the digitized image. For both cameras, data acquisition as well as image conditions were the same as those used in clinical procedures.

### C. Phantom Description

We built breast phantoms to perform SNR analyzes on different tumor sizes. The phantoms consisted of three cylindrical chambers, 8, 10, and 13 cm in diameter and 15 cm in height. We filled each with $^{99m}$Tc-labeled water to a height of 3, 6, and 9 cm to simulate different breast compression thickness. We accounted for three tumor sizes, which corresponded to the clinical staging criteria of T1b, i.e., greater than 5 mm, less than or equal to 1 cm. The T1b hot spots were in 6 mm, 8 mm, and 10 mm diameter cylinders. The tumor depth was 0.5 cm or 3. cm (source-collimator distance—SCD), which we obtained with a tumor support as shown in Fig. 4. We placed a $30 \times 30 \times 20$ cm$^3$ box, which was also filled with $^{99m}$Tc-labeled water, close to the breast phantom to simulate the torso emission (see Fig. 4).

We chose radioactivity concentration values to obtain clinical images with about a 1 : 1 torso : breast ratio (100 nCi/cc concentration). For the tumor phantom, we used a tumor to breast ratio of 30 : 1 for the 6 mm tumor, 10 : 1 for the 8 mm tumor and 8 : 1 for the 10 mm tumor. We chose a high tumor to breast ratio for the 6 mm tumor in order to have an appropriate SNR evaluation for small lesions in all cameras.

### D. Data Acquisition and Method

We performed all measurements by simulating a craniocaudal projection. We analyzed the tumor as a function of its size and the breast's thickness. We are aware that for an Anger camera, the experimental set up does not correspond to the usual scintimammographic technique which is currently performed in the prone position. The aim of this choice was to enhance the AC imaging performance by reducing the tumor-to-collimator distances in order to better evaluate the influences of the intrinsic detector characteristics on tumor SNR values.

We adjusted the data acquisition time to correct for $^{99m}$Tc decay to collect comparable counts per image. We digitized the images from the AC and SPEM camera in the same manner as those collected and used for clinical examination. In particular, we set the AC and SPEM to $3.2 \times 3.2$ mm$^2$ ($128 \times 128$) and $2 \times 2$ mm$^2$, respectively.

In the SGC, the nonuniformity of pulse height affects the overall energy resolution and the energy window selection. To correct for this nonuniformity, we create a look-up table (LUT) using a $^{99m}$Tc flood field irradiation (see Fig. 5). Starting with a flood field image, we define the Regions of Interest (ROIs) so that they contain the same number of counts for each crystal. After a manual selection of the ROI matrix columns, the algorithm calculates the appropriate rows [see Fig. 5(i)] and, fixing a reference gain value, it creates a matrix of gain factors to adjust the gain of the spectrum corresponding to each crystal. The new adjusted total spectrum is shown as **b** in Fig. 5(ii), which should be compared to the unadjusted spectrum [**a** in Fig. 5(ii)]. The last procedure produced an inhomogeneous sensitivity in the flood field, which we correct with an appropriate matrix de-

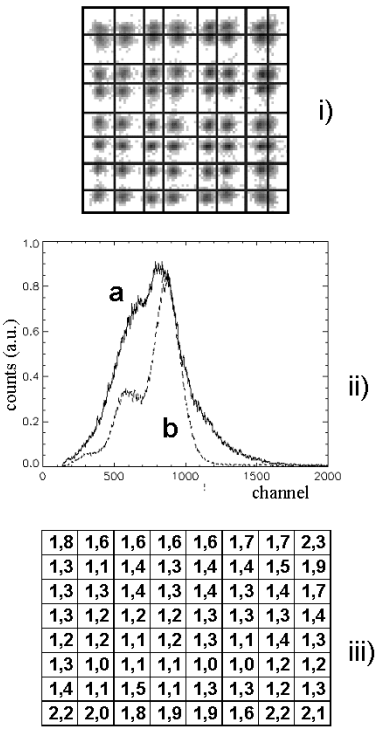


| | | | | | | | |
|---|---|---|---|---|---|---|---|
| 1,8 | 1,6 | 1,6 | 1,6 | 1,6 | 1,7 | 1,7 | 2,3 |
| 1,3 | 1,1 | 1,4 | 1,3 | 1,4 | 1,4 | 1,5 | 1,9 |
| 1,3 | 1,3 | 1,4 | 1,3 | 1,4 | 1,3 | 1,4 | 1,7 |
| 1,3 | 1,2 | 1,2 | 1,2 | 1,3 | 1,3 | 1,3 | 1,4 |
| 1,2 | 1,2 | 1,1 | 1,2 | 1,3 | 1,1 | 1,4 | 1,3 |
| 1,3 | 1,0 | 1,1 | 1,1 | 1,0 | 1,0 | 1,2 | 1,2 |
| 1,4 | 1,1 | 1,5 | 1,1 | 1,3 | 1,3 | 1,2 | 1,3 |
| 2,2 | 2,0 | 1,8 | 1,9 | 1,9 | 1,6 | 2,2 | 2,1 |

Fig. 5. LUT procedure for the $8 \times 8$ pixel array example: (i) pixel identification; (ii) spectra reconstruction: (a) raw spectra, (b) reconstructed spectra; (iii) homogeneity counting factor.

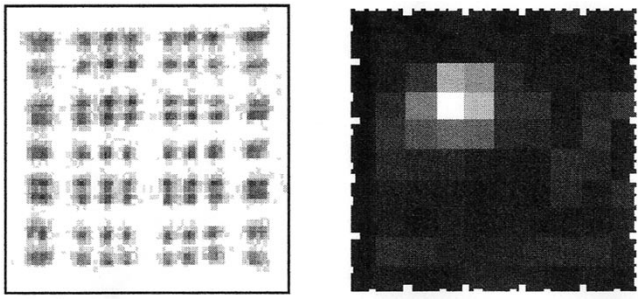

Fig. 6. SGC images obtained by $10 \times 10$ pixel array, 8 cm diameter breast phantom, 3 cm thickness and 6 mm tumor. On the left an image before the correction, on the right the same image after the LUT application.

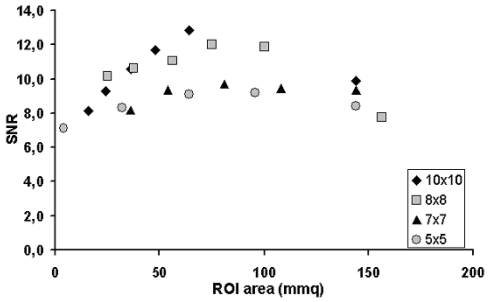


Fig. 7. SNR value versus ROI area for SGC.

rived from the original flood field measurement [see Fig. 5(iii)]. Fig. 6 shows the image of a "tumor" for a pixelated camera taken

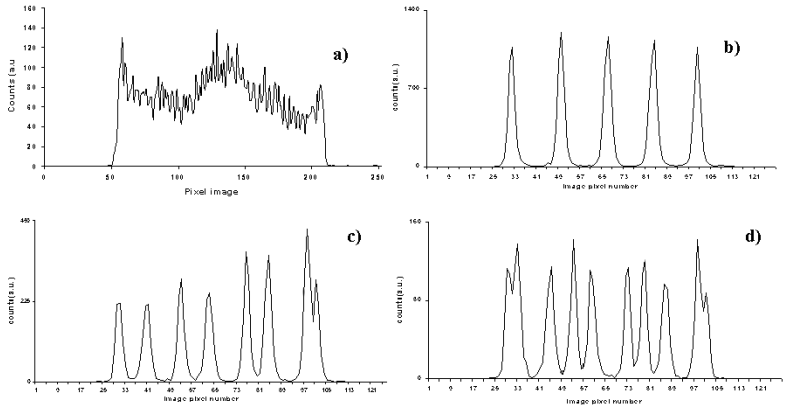


Fig. 8. SPEM and SGC image profile, flood field, with collimator. (a) SPEM image profile; (b) 5 × 5 pixel; (c) 8 × 8 pixel; (d) 10 × 10 pixel.

in high resolution on the left and on the right is the LUT corrected image as a 10 by 10 matrix.

We will calculate the SNR value for the breast phantom with the following formula:

$$\mathrm{SNR} = \frac{\mathrm{SOURCE - BACK}}{\sqrt{\mathrm{SOURCE}}} \tag{1}$$

where SOURCE and BACK are the total number of counts obtained from the ROI containing the tumor and the background, that is, the healthy breast tissue, respectively.

We also investigated SNR values as a function of ROI area and phantom configuration. In Fig. 7 shows the SNR versus ROI area for SGC, for different pixel size. In order to minimize the error on SNR values, due to the low statistics, we also acquired images over time periods which were ten times longer than most clinical studies. We scaled the SNR in order to obtain values corresponding to the actual clinical condition.

### *E. Monte Carlo Simulation*

We used the newest version of the EGS family of Monte Carlo code, i.e., EGSnrc. Simulations included all the physical processes available with EGS, such as Compton and Rayleigh scattering and photoelectric absorption with emission of either fluorescence photons or Auger electrons. We fixed the lower cut-off energy at 5 keV for photons; whereas, we neglected electron transport by assuming that an electron deposits all its energy in its point of interaction. We used this assumption for the entire simulated apparatus, that is, in the breast phantom, the collimator, and in the detector. In order to reduce the computational time, we adopted a modular geometric description for the collimator and the pixelated detector. The simulated breast phantom consisted of a 9 cm diameter cylinder made of breast-equivalent tissue; we simulated three different cylinder lengths, (3, 6, 9 cm), corresponding to three different breast thickness. In order to emulate a clinical examination, we calculated the number of simulated photons for an imaging time of 10 min and a background activity of 100 nCi/cc: the number of 140 keV photons emitted ranged from 420 million to 1.3 billion. We simulated three different spherical tumors (6, 8, 10 mm diameter), located at various depths (0.5, 3 cm from the collimator); we used a tumor to breast ratio of 10 : 1. The simulated camera included a lead collimator and a CsI pixelated detector. We simulated the collimator described in Table I for the SPEM camera. The detector consisted of different 5 mm thick pixelated crystals: the size of a single pixel ranged from 2.0 × 2.0 mm$^2$ to 4.2 × 4.2 mm$^2$; the detector's pixels had no space between them. We considered a 20% FWHM energy resolution for the detector. The final coordinates of a detected photon were at the center of mass of all the pixels with which the photon had interacted [7].

TABLE III
SUMMARY OF RESULTS

| Pixel size mm$^2$ | Energy resolution % FWHM | Photo fraction % FWHM | Flat Uniformity [a] % |
|---|---|---|---|
| 4.2 x 4.2 | 21.3 | 90 | 90 |
| 3 x 3 | 22.0 | 90 | 87 |
| 2.5 x 2.5 | 23.0 | 91 | 81 |
| 2 x 2 | 28.0 | 93 | 71 |

[a] measurements with collimator

## III. RESULTS AND DISCUSSION

We show in Fig. 8(a) the flood field image profiles for SPEM and SGC respectively, for different pixel size. The SPEM image cross section shows a great deal of nonuniformity in sensitivity across the FoV and it is well known that this due to nonlinearity and spatial distortions in this type of camera [8], [9]. A pixellated camera has the possibility of placing close to 100% of the events in the correct pixel [Fig. 8(b)] if the pixels are very large. As the pixels get smaller the task be comes more difficult [Fig. 8(c) and (d)]. The individual elements guide the light down the crystal giving the possibility of better localization. The energy resolution after the LUT application ranged from 21% to 28% FWHM (see Table III). We found the 2 × 2 and 2.5 × 2.5 mm$^2$ pixel arrays to have the worst energy resolution. This result was mainly due to a peripheral nonlinear distortion (clearly visible in Fig. 8) originating from the under-sampling of the anodic light, which in turn compromised good pixel identification. All SGC data were supported by Monte Carlo simulation results.

When the detection system has good pixel identification, one can correct distortions in both the pulse height and spatial broad-

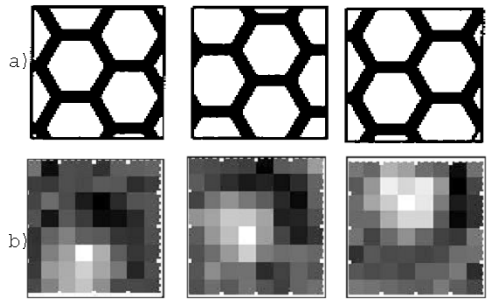


Fig. 9. (a) Effective pixel detection area as a function of the lattice periodicity on 3 mm pixel size. (b) SGC detection area scanning of a breast phantom including 4 mm diameter size tumor.

TABLE IV
AREA FRACTIONS OBSCURED BY COLLIMATOR SEPTA OF SINGLE CRYSTAL PIXEL

| Pixel Size ($mm^2$) | Maximum | Minimum | Average | Stand. dev. |
|---|---|---|---|---|
| 4.2 x 4.2 | 31,3% | 27,5% | 29,3% | 1,9% |
| 3 x 3 | 28,8% | 23,6% | 26,2% | 2,3% |
| 2.5 x 2.5 | 27,9% | 2,7% | 25,0% | 6,0% |
| 2 x 2 | 30,1% | 21,6% | 25,7% | 2,9% |

ening. Consequently, fluctuations on inhomogeneous responses to flood field irradiation ranged from 10% to 30%.

The small area of the SGC or, more exactly, the small number (compared to a larger camera) of pixels available to make an image enhances the effect of the collimator/crystal lattice match on the overall homogeneity of the spatial response (fourth column on Table III). The nonuniform counting response increases as pixel size decreases, making pixel identification more critical. In particular, for $2 \times 2$ $mm^2$ pixels, where the peripheral crystals represent about 40% of the overall crystal area, good pixel identification is essential.

To test the influence of a collimator on a crystal array's counting uniformity, we analyzed the effective pixel detection area as a function of collimator lattice periodicity.

Fig. 9(a) shows three examples of $3 \times 3$ $mm^2$ pixels with different areas filled lead-filling on size. The values of septa area fraction on detection active area are reported in Table IV. Values fluctuations for different pixel size show a standard deviation of about 2% for the largest pixel size and of about 3% for smallest one. 3 mm pixel size represents the worst match between crystal array and collimator lattice. Furthermore to test LUT procedure influence and collimator lattice periodicity on tumor SNR value fluctuation, we utilized a breast phantom 3 cm thick, including 4 mm diameter tumor at 3 cm SCD to scan the SGC detection area. Increasing the usual examination time by a factor of 10, SNR statistical error was minimized. In Fig. 9(b) three images show an example of the results obtained for 3 mm size pixels. Standard deviation of the tumor's SNR was less than 5%. The result can be considered good, if we assume that it includes all errors. We only used the SPEM camera and the Anger camera for the initial test on tumor SNR. We took measurements which included torso together with breast phantom and we used the same acquisition time as in clinical trials. Table V, shows that the measurements are strongly affected by large fluctuations. These are due to low statistics and background introduced by the presence of the torso. To differentiate SNR contribution from

TABLE V
TUMOR SNR FOR SPEM AND ANGER CAMERA

| Brest Thickness (cm) | Tumor fl (mm) | SPEM (2 mm pixel size) | ANGER |
|---|---|---|---|
| 3 | 8 | 14.0± 2.0 | 7.0 ± 3.0 |
| 6 | 8 | 6.0 ± 1.0 | 5.0 ± 2.0 |
| 9 | 8 | 6.0 ± 2.0 | 4.0 ± 2.0- |
| 3 | 10 | 21.0± 5.0 | 20.0 ± 3.0 |
| 6 | 10 | 20. 0 ± 6.0 | 15.0 ± 3.0 |
| 9 | 10 | 17.0 ± 4.0 | 14.0 ± 5.0 |

TABLE VI
TUMOR SNR VALUES

| Breast Thickness (cm) | Tumor fl (mm) | SPEM (2 mm pixel size) | ANGER | SMALL CAMERA Pixel size | | |
|---|---|---|---|---|---|---|
| | | | | 2.0 mm | | 3.0 mm |
| | | | | Experimental Data | Montecarlo Simulation | |
| 3 | 6 | 4.0± 0.2 | 4.0± 0.2 | 13.0 ± 0.7 | 8.8 ± 0.9 | 10.0 ± 0.5 |
| 6 | 6 | - | - | 11.4 ± 0.6 | 7.5 ± 0.8 | 8.9 ± 0.5 |
| 3 | 8 | 18.0± 1.0 | 19.0± 1.0 | 16.0 ± 0.8 | 17.2 ± 1.2 | 16.0 ± 0.8 |
| 6 | 8 | 9.3 ± 0.5 | 10.1± 0.5 | 13.0 ± 0.7 | 14.7 ± 1.0 | 14.6 ± 0.8 |
| 3 | 10 | 31.0± 1.6 | 32.0± 1.6 | 20.0 ± 1.0 | 28.2 ± 3.0 | 25.0 ± 1.2 |
| 6 | 10 | 21.4 ± 1.2 | 22.8± 1.2 | 19.0 ± 0.9 | 24.6 ± 2.5 | 19.6 ± 1.0 |

For all experimental data, the 6 mm tumor has a 30:1 tumor-background ratio, the 8 mm a 10:1 tumor background ration and the 10 mm an 8:1 tumor background ratio. For Montecarlo simulations, all tumors have a 10:1 tumor-background ratio

the tumor and the torso, we studied the breast alone. Table VI summarizes SNR results obtained from different breast thickness and tumor sizes at a distance of 3 cm between tumor and collimator for all of the cameras. AC and SPEM image contrast showed a strong dependence on breast thickness. SNR values decrease at 6 cm breast thickness ranges between 30% and 50% for 10 mm and 8 mm tumor size, respectively. Differences for the 6 mm tumor size results were not detected between the SPEM and Anger camera. For the smallest tumor size, the AC response is depressed and this is due to its poor spatial resolution. In SPEM, the better spatial resolution does not allow improvement of the SNR values that are always under the visibility limit (SNR $= 5$). This can be attributed to its bad spatial uniformity response. On the contrary SGC shows SNR values ranging between 9 and 13. The contrast reduction between 3 cm and 6 cm breast thickness is similar (20%) for all phantom configurations. It also agrees with the Monte Carlo simulation. In particular, the smallest pixel size allows one to obtain a better image spatial resolution and a greater number of pixels available to evaluate the SNR value. This positive effect is probably offset by poorer uniformity in the detector response, which is only partially corrected by the LUT procedure. We can see that the crystal size plays an important role in the detection of small tumors but it must be associated with a good pixel identification scheme. If the events are not placed in the correct pixel, contrast can be severely reduced. This is clearly seen in the comparison of SNR values with Monte Carlo simulations. The experimental SNR values were less than half the comparable values obtained with the Monte Carlo simulation.

AC and SPEM performances were better for the 8 mm tumor and seemed to be comparable to SGC results, which indicates that SNR for tumor size $\geq$8 mm does not depend only on the spatial resolution of the detector. In fact, for SGC there was not any appreciable SNR difference between the 2 mm and 3 mm pixel size.

In Table VII we detailed SGC results obtained for different breast thickness and tumor depths. We obtained the best results using the $2 \times 2$ $mm^2$ pixel configuration, with a 10–15% improvement with respect to the $4.2 \times 4.2$ $mm^2$ pixel size. In Fig. 10, tumor images are shown for the different pixel sizes

TABLE VII
SMALL CAMERA SNR VERSUS TUMOR DEPTH AND BREAST THICKNESS—6 mm TUMOR

| Tumor Depth (cm) | Breast thickness (cm) | Breast Alone Pixel size (mm) | | | | Torso and Breast Pixel size (mm) | | |
|---|---|---|---|---|---|---|---|---|
| | | 4.2 | 3.0 | 2.5 | 2.0 | 4.2 | 3.0 | 2.0 |
| 0.5 | 3 | 12.0±0.6 | 13.0 ± 0.6 | 13.0 ± 0.6 | 15.0± 0.7 | 10.0 ± 0.5 | - | - |
| 3 | 3 | 9.0 ± 0.5 | 10.0 ± 0.5 | 12.0 ± 0.6 | 13.0 ± 0.6 | 7.0 ± 0.5 | - | - |
| 0.5 | 6 | 9.0 ± 0.5 | 10.0 ± 0.5 | 12.0 ± 0.6 | 13.0± 0.6 | 7.0 ± 0.5 | 10.0 ± 0.5 | - |
| 3 | 6 | 7.0 ± 0.4 | 9.0 ± 0.5 | 9.0 ± 0.5 | 11.0 ± 0.5 | 6.0 ± 0.4 | 8.0 ± 0.4 | 10.0 ± 0.5 |

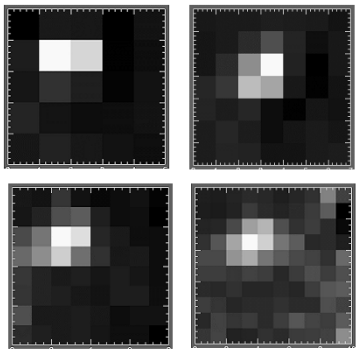

Fig. 10. SGC image for 6 mm tumor at 0.5 cm tumor depth. From upper left corner clockwise: $4.2 \times 4.2\ \text{mm}^2$, $3 \times 3\ \text{mm}^2$, $2.5 \times 2.5\ \text{mm}^2$, and $2 \times 2\ \text{mm}^2$.

investigated. In Table VII are also shown some data obtained including torso at 5 cm tumor distance. We must keep in mind that SNR values are mean values, which decrease as the tumor-torso distance decreases.

## IV. CONCLUSION

In this paper, we investigated potential methods for enhancing SNR in scintimammography offered by a new generation of PSPMTs coupled to scintillator arrays, for small tumor imaging. Starting with very good crystal pixel identification, we generated a correspondence between image digitization and scintillation crystal lattice. We calculated SNR values for different combinations of scintillation pixel size, tumor size, and breast thickness. Finally, we compared our SGC results to the results obtained from the Anger camera and a dedicated SPEM imager. The results showed how the SGC improved, up to a factor of three, the SNR of a 6 mm tumor with 2 mm scintillation pixel size. Furthermore, the SGC improved the contrast of the image for 6 cm breast thickness Additionally, the smallest crystal pixel size provided the highest tumor SNR for small tumors.

We obtained comparable SNR results for 8 mm and 10 mm tumors from the three detectors. Preliminary data seemed to confirm the higher contrast capability of the proposed new camera, but further results are needed to completely validate the procedure. We found that the main limitation of the SGC was the small size of its active area, which makes it critical to measure its effectiveness with large tumors. Future work will include study on new NaI(Tl) scintillating arrays to improve pixel identification with large area PSPMTs and with new PSPMT flat panel Hamamatsu H8500.

## REFERENCES

[1] J. A. Khalkhali *et al.*, "Scintimammography: The complementary role of $^{99m}$Tc, sestamibi prone breast imaging for the diagnosis of breast carcinoma," *Radiol.*, vol. 196, no. 2, pp. 412–426, 1995.
[2] R. Pani *et al.*, "Dedicated gamma camera for single photon emission mammography (SPEM)," *IEEE Trans. Nucl. Sci.*, vol. 45, pp. 3127–3133, Dec. 1998.
[3] R. Pani *et al.*, "Portable gamma camera for clinical use in nuclear medicine," in *Proc. IEEE Nuclear Science Symp. Conf. Record*, vol. 2, Anaheim, CA, 1996, pp. 1170–1174.
[4] S. Majewski *et al.*, "Optimization of dedicated scintimammography procedure using detector prototypes and compressible phantoms," *IEEE Trans. Nucl. Sci.*, vol. 48, pp. 822–829, June 2001.
[5] F. Scopinaro *et al.*, "High resolution scintimammography improves the accuracy of $^{99m}$Tc methoxyisobubylisonitrile scintimammography: Use of a new dedicated gamma camera," *Eur. J. Nucl. Med.*, vol. 26, no. 10, Oct. 1999.
[6] "R7600-C8 Position sensitive photomultiplier," Hamamatsu technical data sheet.
[7] F. Bevilacqua, D. Bollini, R. Campanini, M. Gombia, N. Lanconelli, and A. Riccardi, "A modular description for collimator geometry in EGS simulation tasks," in *Proc. IEEE NSS/MIC Conf. Rec. 2001*, vol. 3, Nov. 2001, pp. 1303–1305.
[8] G. Muehllehner, J. G. Closher, and E. W. Stoub, "Correction for field Nonuniformity in scintillation cameras through removal of spatial distortion," *J. Nucl. Med.*, vol. 21, no. 8, pp. 771–776, 1980.
[9] D. E. Persyk, J. Morales, R. McKeighen, and G. Muehllehner, "The quadrant photomultiplier," *IEEE Trans. Nucl. Sci.*, vol. NS-26, pp. 364–267, Feb. 1979.